






Article

Crystal Structures of Antiarrhythmic Drug Disopyramide and Its Salt with Phthalic Acid

Majid Ismail Tamboli ^{1,†}, Yushi Okamoto ¹, Yohei Utsumi ¹, Takayuki Furuishi ^{1,†} , Siran Wang ¹, Daiki Umeda ¹, Okky Dwichandra Putra ^{1,*} , Kaori Fukuzawa ¹ , Hidehiro Uekusa ²  and Etsuo Yonemochi ^{1,*} 

¹ Department of Physical Chemistry, School of Pharmacy and Pharmaceutical Sciences, Hoshi University, 2-4-41 Ebara, Shinagawa-ku, Tokyo 142-8501, Japan; t-majid@hoshi.ac.jp (M.I.T.); m1903@hoshi.ac.jp (Y.O.); s172504@hoshi.ac.jp (Y.U.); t-furuishi@hoshi.ac.jp (T.F.); m1936@hoshi.ac.jp (S.W.); m1802@hoshi.ac.jp (D.U.); k-fukuzawa@hoshi.ac.jp (K.F.)

² Department of Chemistry, School of Science, Tokyo Institute of Technology, Tokyo 152-8551, Japan; uekusa@chem.titech.ac.jp

* Correspondence: dwichandraputra@yahoo.com (O.D.P.); e-yonemochi@hoshi.ac.jp (E.Y.); Tel.: +81-3-5498-5148 (O.D.P.); +81-3-5498-5048 (E.Y.)

† Co-first author, these authors contributed equally to this work.

Abstract: Disopyramide (DPA) is as a class IA antiarrhythmic drug and its crystallization from cyclohexane at ambient condition yields lower melting form crystals which belong to the monoclinic centrosymmetric space group $P2_1/n$, having two molecules in an asymmetric unit. Crystal structure analysis of pure DPA revealed closely associated DPA molecules aggregates via amide–amide dimer synthon through the N–H···O hydrogen bond whereas the second amide hydrogen N–H engaged in an intramolecular N–H···N hydrogen bond with N-nitrogen of 2-pyridine moieties. Crystallization of DPA and phthalic acid (PA) in 1: 1 stoichiometric molar ratio from acetone at ambient condition yielded block shape crystals of 1:1 DPA_PA salt. Its X-ray single crystal structure revealed the formation of salt by transfer of acidic proton from one of the carboxylic acidic groups of PA to the tertiary amino group of chain moiety (N3-nitrogen atom) of DPA molecules. DPA_PA salt crystals belong to the monoclinic centrosymmetric space group $P2_1/n$, comprising one protonated DPA and one PA[−] anion (hydrogen phthalate counterion) in an asymmetric unit and linked by N–H···O and C–H···O hydrogen bonds. Pure DPA and DPA_PA salt were further characterized by differential calorimetric analysis, thermal gravimetric analysis, powder x-ray diffraction and infrared spectroscopy.

Keywords: disopyramide; phthalic acid; salt; crystal structure; metastable



Citation: Tamboli, M.I.; Okamoto, Y.; Utsumi, Y.; Furuishi, T.; Wang, S.; Umeda, D.; Putra, O.D.; Fukuzawa, K.; Uekusa, H.; Yonemochi, E. Crystal Structures of Antiarrhythmic Drug Disopyramide and Its Salt with Phthalic Acid. *Crystals* **2021**, *11*, 379. <https://doi.org/10.3390/cryst11040379>

Academic Editor:

Duane Choquesillo-Lazarte

Received: 27 February 2021

Accepted: 30 March 2021

Published: 6 April 2021

Publisher's Note: MDPI stays neutral with regard to jurisdictional claims in published maps and institutional affiliations.



Copyright: © 2021 by the authors. Licensee MDPI, Basel, Switzerland. This article is an open access article distributed under the terms and conditions of the Creative Commons Attribution (CC BY) license (<https://creativecommons.org/licenses/by/4.0/>).

1. Introduction

Recent past literature related to crystal engineering revealed that there is an intensification of interest in the preparation, crystallization, solid-state characterization and the studying of the X-ray single-crystal structure of active pharmaceutical ingredients (APIs) and their novel solid forms that includes polymorph [1–5], multi-component crystal such as cocrystals [6–8], salt [9], and solvate [10–14] due to their potential applications in the improvement of physicochemical properties of APIs such as solubility [15–17], stability [18–20], hygroscopicity [21], bioavailability [22–24] and so on. Further, advancement in this research area directed towards the understanding crystal–structure, studying supramolecular synthons, hydrogen/halogen bonding interaction and other various non-covalent interactions within them [25–27] as well as correlating structure with the physicochemical properties [28–32]. These structure-property relation studies are helpful and encourage many researchers towards designing and synthesis of new functional molecular solids, and multi-component complexes of APIs, and other molecular entities with desirable and specific chemical or physical properties [33–38].

Disopyramide (2-diisopropylaminoethyl)-phenyl-2-pyridineacetamide (DPA) was developed [39] as a class IA antiarrhythmic drug with a pharmacological profile of action similar to that of quinidine and procainamide in that targets sodium channels to inhibit conduction [40,41]. Currently, DPA and $[C_{21}H_{30}N_3O]^+[H_2PO_4]^-$ disopyramide dihydrogen phosphate are intravenously and orally administered for clinical use. DPA displaying polymorphism behavior and two solid forms were reported in the literature and named as a low-melting type crystal (85–87 °C) and a high-melting type crystal (95–98 °C) [42]. Of the two crystal forms, the high melting point type crystal is thermodynamically stable, and the low melting point type crystal is easily converted to the high melting point type crystal [42]. However, single-crystal X-ray data of either of crystal form were not present in the Cambridge Structural Database (CSD), whereas the crystal structure of $[C_{21}H_{30}N_3O]^+[H_2PO_4]^-$ disopyramide dihydrogen phosphate has been reported by Kawamura and Hirayama in 2011 [43]. Furthermore, X-single crystal structure of (+)-disopyramide (2R,3R)-bitartrate salt was reported in 1980 for determining the absolute configuration of disopyramide by Burke and Nelson [44], and the structure was not present in the CSD. Moreover, to the best knowledge of the authors, not much research has been carried out with respect to creating the novel salt form of DPA.

DPA has asymmetric carbon marked by a star that is connected to four different groups shown in Figure 1a. It has a flexible molecular framework as well as the presence of a hydrogen bond donor and acceptor site, and hence there will be a high possibility to form multicomponent crystals. Thus, it could be the potential candidate in exploring its different conformational modification by obtaining X-ray single crystal structures of different solid forms of DPA.

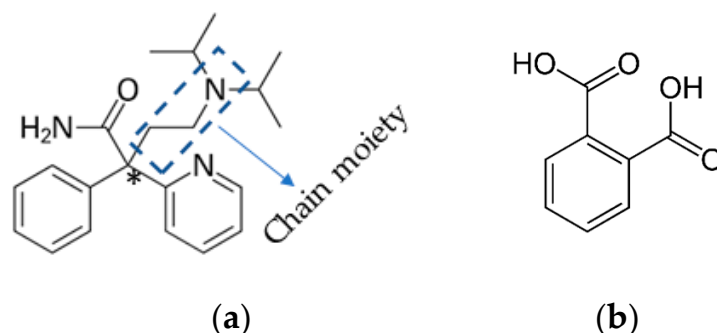


Figure 1. Structures of (a) racemic disopyramide (DPA) and (b) phthalic acid (PA).

We are going to focus on the crystallization and crystal engineering research on active pharmaceutical ingredients (APIs), particularly on improving the physicochemical properties of drug molecules by undertaking polymorphic study [45], making multicomponent crystals [46], such as its solvates [47], cocrystals [48], and salts [49]. In this report, we discuss the X-ray single-crystal structure of the lower melting temperature form of DPA and novel DPA_PA salt [Phthalic acid (PA), Figure 1b], detailed crystal structure analysis and its characterization.

2. Materials and Methods

2.1. Materials

DPA and PA were purchased from Tokyo Chemical Industry Co. Ltd. (Tokyo, Japan). All other analytical-grade solvents and reagents were commercially obtained and used without further purification.

2.2. Crystallization

2.2.1. DPA

The minimum amount of solvent cyclohexane was used to dissolve the DPA by sonication at 25 °C; it was then immediately filtered and the resulting solution was maintained at ambient temperature for 1–2 days, yielding a colorless block-shaped crystal.

2.2.2. DPA_PA Salt for Single X-ray Crystal Structure Analysis

DPA and PA were each taken in a molar ratio of 1:1, suspended in diethyl ether and stirred at 25 °C and 170 rpm (IKA Plate_RCT 4, IKA, IKA® Japan K.K., Osaka, Japan) for 5 days. After that, the precipitated material was recrystallized in acetone, yielding a colorless block-shaped crystal.

2.2.3. DPA_PA Salt for Characterization (PXRD, DSC, IR, and TG)

DPA (0.5 mmole) and PA (0.5 mmole) in a 1:1 molar ratio was grinded in a mortar and pestle for about 10 min to become a fine powder, then a few drops of acetone were added to it, then again grinded for 10–15 min to obtain powder. From this grinded material, 150 mg was used for the crystallization experiment. Colorless crystals were obtained on the side wall of the vial by upon dissolving the 150 mg grinded material in 20 mL acetone under sonication at a temperature 30 °C for 10 min; the resulting solution obtained after filtration was left for slow evaporation at ambient condition for 3–4 days.

2.3. Single-Crystal X-ray Diffraction

The single-crystal X-ray diffraction data for DPA and DPA_PA salt were collected at 93 K. The measurements were carried out in ω -scan mode with an R-AXIS RAPID II (Rigaku Co., Tokyo, Japan) using the Cu-K α X-ray obtained from rotating the anode source with a graphite monochromator. The integrated and scaled data were empirically corrected for absorption effects using ABSCOR [50,51]. The initial structure was solved using the direct method with SIR 2004 and refined on F^2 with SHELXL 2014 [52,53]. All non-hydrogen atoms were refined anisotropically. The hydrogen atom attached to the nitrogen N2 and N5 atom in pure DPA and the hydrogen atom attached to the nitrogen N2 as well as hydrogen H5A present in between the O3 and O5 oxygen in the DPA_PA salt were located using the differential Fourier map and refined isotropically. All other hydrogen atom positions were calculated geometrically and included in the calculation using the riding atom model; the calculations were performed for all the hydrogen atoms. Moreover, in the DPA_PA salt, protonated DPA molecules display disordered structure in which two molecules with opposite configuration share the same site. Their occupancies were fixed to 0.5.

The molecular graphics were produced using Mercury 4.1.0 software [54]. CCDC 2065231 contains the supplementary crystallographic data for the DPA and CCDC 2065230 contains the supplementary crystallographic data for the DPA_PA salt, and can be obtained free of charge from the Cambridge Crystallographic Data Centre via www.ccdc.cam.ac.uk/data_request/cif (accessed on 2 April 2021).

2.4. Powder X-ray Diffraction (PXRD)

The PXRD patterns of all samples were measured in the reflectance mode using a SmartLab diffractometer (Cu K α source (40 kV and 200 mA), D/teX ultra-high-speed position-sensitive detector, Rigaku). Diffraction patterns (2θ) were collected from 5° to 40° at 25 °C with a step of 0.01° and a scan speed of 20°/min.

2.5. Differential Scanning Calorimetry (DSC) and Thermogravimetric (TG) Measurements

DSC and TG measurements were carried out with the Thermo plus EVO2-DSC 8230 and the Thermo plus EVO2-TG8120 TG-DTA, respectively (Rigaku). The DSC sample (~3 mg) was placed in an aluminum-crimped pan, measured at a speed of 5 °C/min from 25 to 250 °C under nitrogen gas (flow rate = 50 mL/min). The TG sample (~10 mg) was

placed into an aluminum-open pan, respectively, and measured at a speed of 5 °C/min from 25 to 250 °C under nitrogen gas (flow rate = 50 mL/min for DPA, PA and 100 mL/min for DPA_PA salt).

2.6. Fourier Transform Infrared Spectroscopy (FT-IR)

The infrared spectra of samples were obtained using FT-IR (FT-IR-4200 spectrometer, JASCO Co., Tokyo, Japan) with an attenuated total reflection (ATR) unit (ATR-PRO 670H-S, JASCO Co.). The spectrum recorded represents an average of 64 scans obtained with a resolution of 4 cm⁻¹ at room temperature. The spectra were collected in the wavenumber ranging from 4000 to 400 cm⁻¹. The internal reflectance element used in this study was a diamond trapezoid having 45° entrance and exit faces.

3. Results and Discussion

3.1. Crystal Structure of DPA

Suitable crystals of DPA were grown from the cyclohexane solvent by slow evaporation at ambient conditions. Its structure was determined by single crystal X-ray diffraction and showed that it crystallized in monoclinic centrosymmetric space group $P2_1/n$, containing two symmetry independent molecules (designated as A and B molecules) in the asymmetric unit and which have opposite configuration. The Oak Ridge Thermal Ellipsoid Plot (ORTEP) of DPA is shown in Figure 2a. In the structural overlay studies two conformers which, having similar configuration, are used and reveal a minor conformational difference at the amide group, phenyl and 2-pyridine moieties, whereas difference at *iso*-propyl moiety was found to be more as shown in Figure 2b. Furthermore, interestingly in both molecules A and B of DPA, the phenyl ring moiety is nearly coplanar with the chain moiety (excluding the *iso*-propyl moiety) whereas the 2-pyridine moiety is oriented nearly perpendicular to the planar part as shown in Figure 2b. The crystallographic information and geometrical parameters for the hydrogen bonding interaction are summarized in Tables 1 and 2.

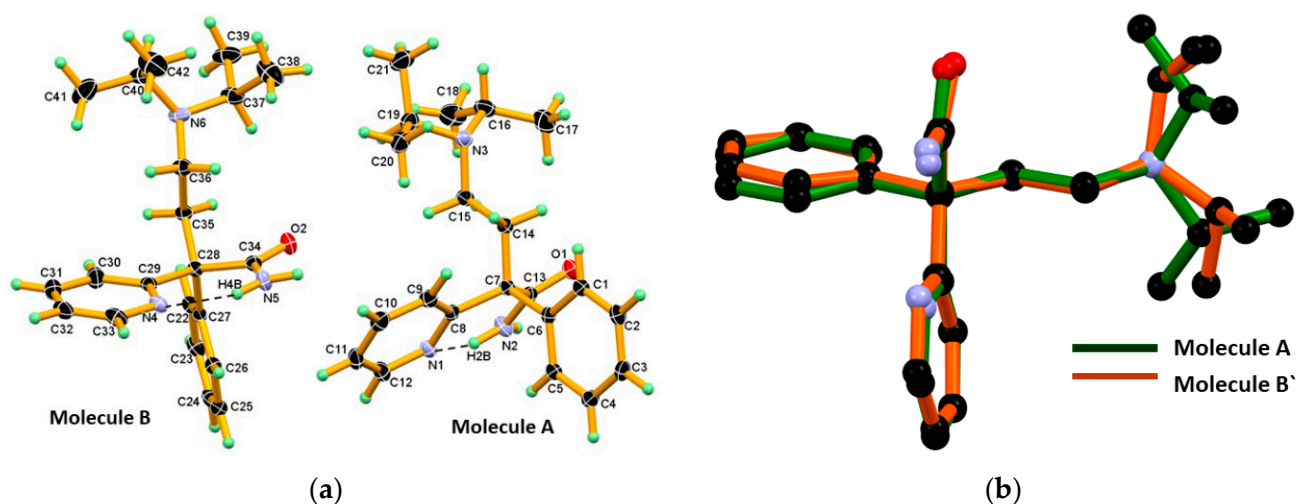


Figure 2. (a) The Oak Ridge Thermal Ellipsoid Plot (ORTEP) diagram of Molecule A and Molecule B of DPA, showing the atom numbering scheme in. Thermal ellipsoid drawn at 50% probability level, and H-atoms are shown as small spheres with arbitrary radii. Both symmetry independent molecules A and B in the asymmetric unit display the N-H...N intramolecular hydrogen bond in $S^1_1(6)$ motif; (b) Structural overlay of two conformers in DPA which, having similar configuration, reveal considerable conformational differences at the *iso*-propyl moiety present on the tertiary N-atom of chain moiety. Molecule B' is inversion symmetry related to Molecule B.

Table 1. Crystallographic data table for the DPA and DPA_PA salt.

Parameters	DPA	DPA_PA
Empirical formula	C ₂₁ H ₂₉ N ₃ O	C ₂₉ H ₃₅ N ₃ O ₅
Formula weight	339.47	505.60
Temperature [K]	93(2)	93(2)
Wavelength [Å]	1.54187	1.54187
Crystal system	Monoclinic	Monoclinic
Space group	<i>P</i> ₂ ₁ / <i>n</i>	<i>P</i> ₂ ₁ / <i>n</i>
Unit cell dimensions		
<i>a</i> [Å]	17.2970 (3)	14.2741 (4)
<i>b</i> [Å]	10.7861 (2)	7.8827 (2)
<i>c</i> [Å]	21.4831 (4)	23.5355 (7)
α [°]	90	90
β [°]	99.385 (7)	91.428 (6)
γ [°]	90	90
Volume[Å ³]	3954.39 (15)	2647.35 (13)
Z and Z'	4, 2	4, 1
Density (calculated) [g/cm ³]	1.140	1.269
Absorption coefficient [mm ⁻¹]	0.552	0.705
F (000)	1472	1080.0
Crystal size [mm x mm x mm]	0.247 × 0.231 × 0.221	0.49 × 0.47 × 0.23
Theta range for data collection [°]	3.048 to 68.192	3.582 to 68.188
Index ranges	−20 ≤ <i>h</i> ≤ 20, −12 ≤ <i>k</i> ≤ 12, −25 ≤ <i>l</i> ≤ 25	−17 ≤ <i>h</i> ≤ 17, −9 ≤ <i>k</i> ≤ 9, −28 ≤ <i>l</i> ≤ 28
Reflections collected	44379	29013
Independent reflections	7200 [R _{int} = 0.0215, R _{sigma} = 0.0129]	4847 [R _{int} = 0.0412, R _{sigma} = 0.0326]
Completeness to theta = 67.687°	99.9%	100%
Absorption correction	Semi-empirical from equivalents	Semi-empirical from equivalents
Max. and min. transmission	0.873 and 0.711	0.850, 0.513
Refinement method	Full-matrix least-squares on F ²	Full-matrix least-squares on F ²
Data/restraints/parameters	7200/0/475	4847/0/350
Goodness-of-fit on F ²	1.052	1.079
Final R indices [I>2σ(I)]	R ₁ = 0.0416, wR ₂ = 0.1024	R ₁ = 0.0434, wR ₂ = 0.1123
R indices (all data)	R ₁ = 0.0435, wR ₂ = 0.1040	R ₁ = 0.0489, wR ₂ = 0.11659
Δρ _{max} , Δρ _{min} (e·Å ⁻³)	0.424 and −0.215	0.265/−0.171

Table 2. Geometrical parameters of the hydrogen bond interaction in DPA and DPA_PA salt.

D-H...A	D-H (Å)	H...A (Å)	D...A (Å)	D-H...A (°)	Symmetry Codes
DPA					
N2-H2B...N1	0.887 (17)	1.965 (17)	2.7006 (16)	139.5 (14)	Intramolecular
N2-H2A...O2	0.890 (16)	2.025 (16)	2.8959 (15)	166.2 (14)	− <i>x</i> + 3/2, <i>y</i> − 1/2, − <i>z</i> +1/2
N5-H4B...N4	0.887 (17)	1.970 (17)	2.7035 (16)	139.1 (14)	Intramolecular
N5-H4A...O1	0.890 (17)	2.046 (17)	2.9286 (14)	171.1 (14)	− <i>x</i> + 3/2, <i>y</i> + 1/2, − <i>z</i> +1/2
C2-H2...O2	0.95	2.677	3.605	165.71	− <i>x</i> + 3/2, <i>y</i> − 1/2, − <i>z</i> +1/2
C10-H10...O2	0.95	2.62	3.3855(15)	138	<i>x</i> , <i>y</i> , <i>z</i>
C11-H11...C _g 4	0.95	2.98	3.7910(13)	145	<i>x</i> , <i>y</i> , <i>z</i>
C32-H32...C _g 2	0.95	2.90	3.7631(13)	152	−1 + <i>x</i> , <i>y</i> , <i>z</i>
C42-H42A...C _g 4	0.98	2.93	3.6320(18)	129	1/2 − <i>x</i> , 1/2 + <i>y</i> , 1/2 − <i>z</i>

C_g2 centroid of the ring (C1-C2-C3-C4-C5-C6), C_g4 centroid of the ring (C22-C23-C24-C25-C26-C27) of molecule A and molecule B of DPA respectively

Table 2. Cont.

D-H...A	D-H (Å)	H...A (Å)	D...A (Å)	D-H...A (°)	Symmetry Codes
DPA_PA salt					
N2-H2A...O4	0.88 (2)	2.02 (2)	2.895 (2)	174 (19)	x, y, z
N2-H2B...O1	0.920 (18)	2.071 (18)	2.9910 (17)	177.8 (18)	$-x, 2 - y, 1 - z$
N3-H3A...O2	1.00	1.72	2.7159 (16)	173	$-1/2 + x, 3/2 - y, 1/2 + z$
O5-H5A...O3	1.11(2)	1.30 (2)	2.4047 (19)	172 (2)	Intramolecular
C2-H2...O1	0.95	2.52	3.4269 (19)	159	$-x, 1 - y, 1 - z$
C9-H9...O4	0.95	2.36	3.294 (2)	167	x, y, z
C15-H15B...N1	0.99	2.57	3.078 (2)	112	Intramolecular
C17-H17C...O1	0.98	2.54	3.4952 (19)	166	Intramolecular
C22-H22...O2	0.95	2.33	2.674 (2)	101	Intramolecular
C25-H25...O4	0.95	2.33	2.688 (2)	101	Intramolecular
C17-H17A...O2	0.98	2.685	3.359 (2)	126.23	$-1/2 + x, 3/2 - y, 1/2 + z$
C14-H14B...O2	0.99	2.603	3.0812(18)	109.73	$-1/2 + x, 3/2 - y, 1/2 + z$
C11-H11...O2	0.95	2.711	3.519	143.35	$1 - x, 2 - y, 1 - z$
C18-H18A...C _g 5	0.98	2.93	3.6222(18)	129	$-x, 1 - y, 1 - z$
C29-O4... C _g 2		3.4808 (16)		146.59 (14)	x, y, z
C29-O4... C _g 3		3.4808 (16)		146.59 (14)	x, y, z

C_g2 centroid of the ring (C1-C3-C2-C1A-C6-C5), C_g3 centroid of the ring (N1-C2-C3-C1-C5-C6) of disordered protonated DPA, C_g5 centroid of the ring (C22-C23-C24-C25-C26-C27) of PA⁻ anion in the DPA_PA salt

In the crystal structure of pure DPA, two closely associated DPA molecules, that is, molecules A and B aggregate via amide homodimer through N-H...O hydrogen bonds, namely N2-H2A...O2, N5-H4A...O1 hydrogen bonds involving amide hydrogen N-H and amide C=O oxygen from both DPA molecules resulting R₂²(8) ring motifs involving two donor and two acceptor atoms. Whereas second amide hydrogen N-H in both symmetry independent DPA molecules formed an intramolecular N-H...N hydrogen bond with the N-nitrogen atom of 2-pyridine moiety in S₁¹(6) motif, namely N2-H2B...N1 and N5-H4B...N4, and hence it controls orientation of 2-pyridine moiety of DPA molecules in the crystal structure as shown in the Figure 3.

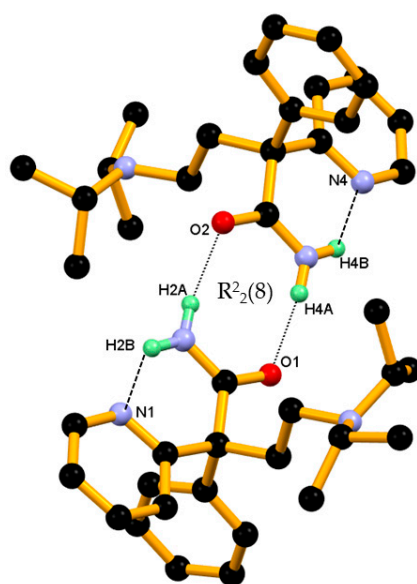


Figure 3. Two closely associated molecules of DPA, that is, molecules A and B involved in ring formation (basic dimeric unit) through an N-H...O hydrogen bond and the resulting R₂²(8) ring motifs. A second amide hydrogen N-H engaged in intramolecular hydrogen bonding with the N-atom of the 2-pyridine moiety in S₁¹(6) motif. Dotted lines indicate the non-covalent interaction (hydrogen atoms not involved in the hydrogen bonding were removed for clarity).

Packing of the dimeric unit down the *c*-axis, resulting in a 1-D chain of the dimeric unit along the *ab*-diagonal, wherein dimeric units of DPA are linked through C-H...O and C-H... π interaction, containing alternate arrangements of vertically and horizontally oriented dimeric units. In this association C10-H10, C11-H11 hydrogen of 2-pyridine moiety of molecule A and C32-H32 hydrogen of 2-pyridine moiety, and C42-H42A hydrogen of *iso*-propyl moiety of molecules B are involved in the alternate C10-H10...O2, C11-H11...C_g4, and C32-H32...C_g2, C42-H42A...C_g4 interaction shown Figure 4a. The dimeric unit assembled helically along the *b*-axis to form a helical chain of the dimeric unit as shown in Figure 4b and dimeric unit along the *b*-axis linked through longer and roughly linear C2-H2...O2 (H2...O2, 2.67 Å, Angle 165.71°) interaction.

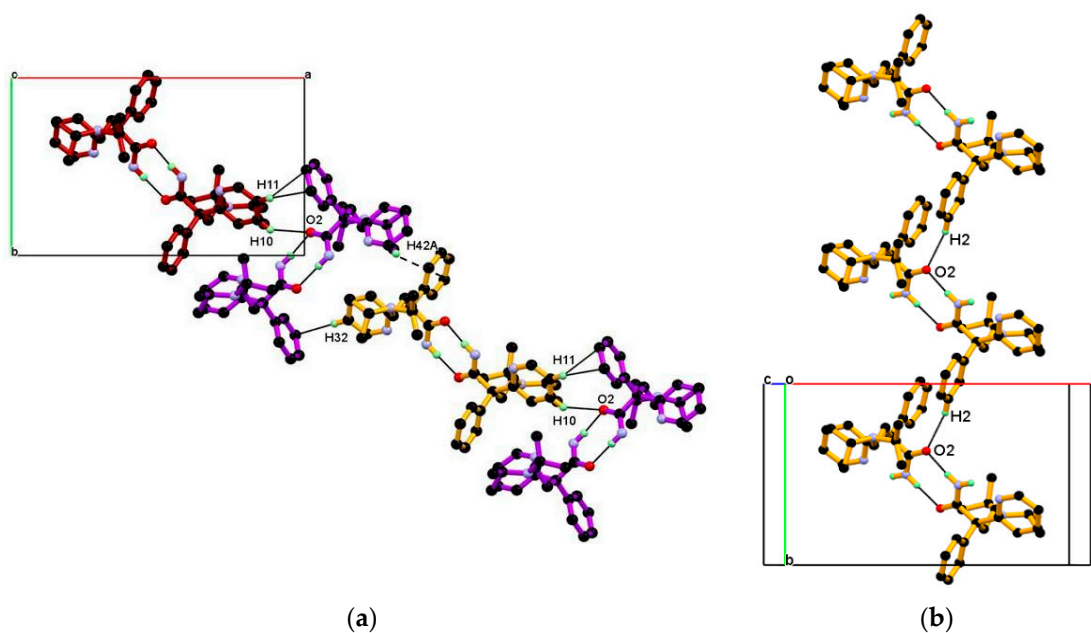


Figure 4. (a) Packing view of the dimeric unit down the *c*-axis, resulting in a 1-D chain of dimeric unit containing an alternate arrangement of vertically and horizontally oriented dimeric unit along the *ab*-diagonal; they are associated through alternate C10-H10...O2, C11-H11...C_g4, and C32-H32...C_g2, C42-H42A...C_g4 interaction and (b) Packing of dimeric unit along the *b*-axis resulting in a helical chain of the dimeric unit, linked through C2-H2...O2 interaction.

Combining the above mentioned packings resulted in the 2-D packing of the dimeric unit in the *ab*-plane, as shown Figure 5. In this packing, the neighboring helical chain of the dimeric unit packed in the *ab*-plane through the alternate C10-H10...O2 C11-H11...C_g4, and C32-H32...C_g2, C42-H42A...C_g4 interaction generate the 2-D packing of the dimeric unit in the *ab*-plane, as shown in Figure 5.

Furthermore, such 2-dimensional structure of the dimeric unit assembled loosely due to the absence of strong interaction along the *c*-axis. In this direction, that is, along the *c*-axis, the 2-D network of dimeric units interact with each other by weak non-covalent interactions and hydrophobic forces between adjacent phenyl and *iso*-propyl groups and such packing of dimeric unit in the *ac*-plane creates a solvent assessable void of size 54.85 Å³ per unit cell and 1.4% of unit cell volume, calculated by using contact surface from Mercury 2020, 2.0 software [54] shown in Figure 6. Crystal with assessable solvent void is recently reported in [55].

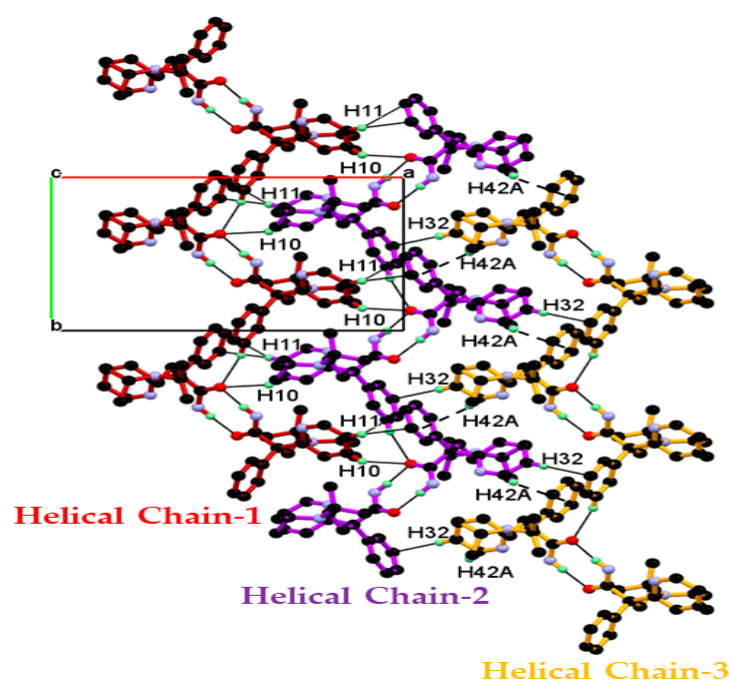


Figure 5. Helical 1-D chain of dimeric unit of DPA is assembled in the *ab*-plane resulting in 2-D packing. In this packing, the central 1-D dimeric unit chain of DPA molecules is associated with the neighboring dimeric chain via C-H \cdots O and C-H \cdots π interaction and the resulting tight packing in the *ab*-plane.

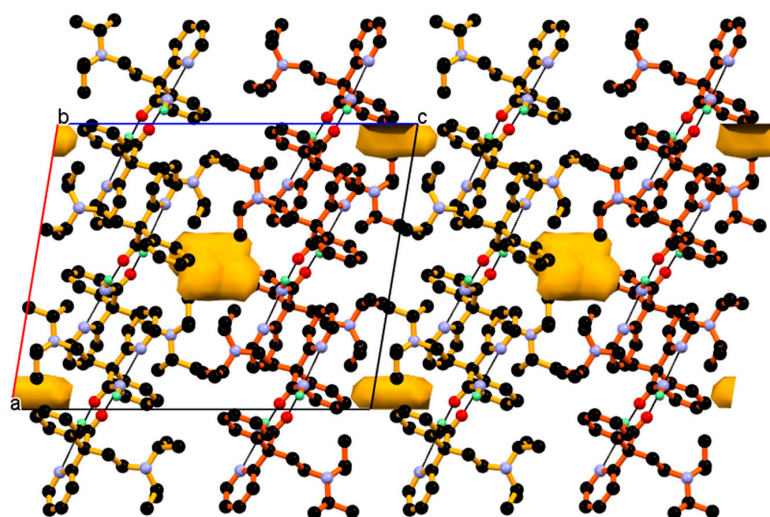


Figure 6. Neighboring 2-dimensional network of dimeric units of DPA assembled loosely via relatively weak non-covalent interaction and hydrophobic forces along the *c*-axis, resulting in 3-dimensional packing; such packing creates a solvent accessible void between them.

3.2. Crystal Structure of DPA_PA Salt

DPA and PA in the 1: 1 stoichiometric molar ratio were crystallized from acetone at ambient condition to obtain a colorless block shape crystal. The ΔpK_a difference between DPA (pK_a : 8.36) and coformer PA (pK_a : 2.94, 5.41) is more than 3 and salt formation was expected based on the basic rule of three [56]. The X-ray single-crystal structure confirmed the formation of DPA_PA salt with approximately similar C–O bond lengths C28–O2, 1.2438 (18), C28–O3, 1.2676 (19) Å) of the (COO $^-$) carboxylate group of PA. These approximate

similarities in the bond length of C–O confirmed the transfer of an acidic proton from one of the carboxylic acid group of PA to the N3-nitrogen atom of the tertiary amino group (chain moiety) of DPA. DPA_PA salt crystallized in the monoclinic centrosymmetric $P2_1/n$ space group comprising one protonated DPA and one PA^- anion in an asymmetric unit, revealing the molecular salt in the 1:1 molar ratio. In the crystal structure of DPA_PA salt, protonated DPA molecules displayed positional disorder and ratio fixed 0.5/0.5 for the two disordered components. DPA is a racemic compound consisting of R and S configurations. These two racemic components R and S are found to occupy the same site with 0.5 and 0.5 occupancy in DPA_PA. In this disorder model, phenyl and pyridine ring were exchanged between R and S, and the other part of DPA molecule was completely overlapped in DPA_PA salt. (Figure 7a).

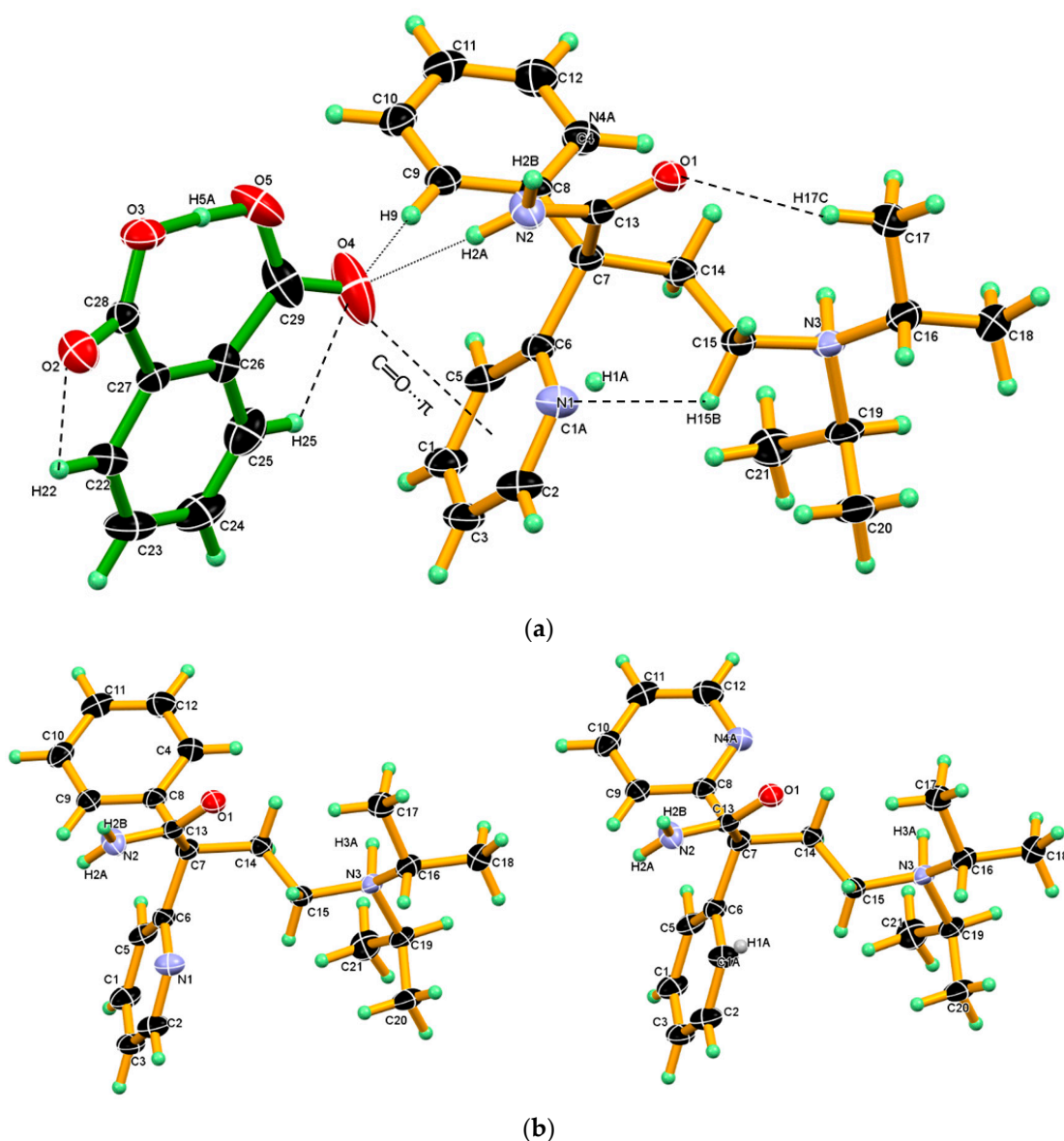


Figure 7. (a) ORTEP diagram of DPA_PA salt, showing the atom numbering scheme wherein C1, N4A and N1, and C1A share the same position. Thermal ellipsoid drawn at 50% probability level, and H-atoms are shown as small spheres with arbitrary radii. DPA_PA salts, displaying intramolecular hydrogen bonds O5-H5A...O3, C17-H17C...O1, C22-H22...O2, C25-H25...O4, C15-H15B...N1 and intermolecular hydrogen bonds N2-H2A...O4 and C9-H9...O4, C=O... π between the salt pair. (b) The disordered DPA molecule in salt crystal. R and S configuration molecules occupied the same site with 0.5 and 0.5 occupancy.

A similar phenomenon was also observed in the crystal structure of ketoconazole [57]. Interestingly, in the one configuration, the phenyl ring is roughly coplanar with chain moiety (excluding the *iso*-propyl moiety), whereas in other configuration, the 2-pyridine moiety is roughly coplanar with the chain moiety (excluding the *iso*-propyl moiety). (Figure 7b).

Both the component in the asymmetric unit, that is, protonated DPA and PA[−] anion linked by strong N2–H2A···O4 hydrogen bond and C9–H9···O4 hydrogen bonds and such assembly in salt facilitated the formation C=O···π interaction between the carboxyl C=O4 of PA[−] anion and phenyl ring Cg2 in one configuration/2-pyridine ring Cg3- in other configuration. In the crystal structure of salt, PA[−] displaying an intramolecular strong O5–H5A···O3 hydrogen bond in which hydroxyl (O5–H5A) of the carboxyl group of the PA[−] anion donates H5A hydrogen intramolecularly to an O3-oxygen atom of the carboxylate group of the PA[−] anion and other C–H···O intramolecular hydrogen bonds namely, C22–H22···O2, C25–H25···O4 present in PA[−] anion and C17–H17C···O1, C15–H15B···N1 in protonated DPA which stabilize the conformation the salt as shown in Figure 7a. The crystallographic information and geometrical parameters for the hydrogen bonding interaction are summarized in Tables 1 and 2.

Hereafter, one conformer of disordered protonated DPA molecule used for discussion of crystal structure and packing of DPA_PA salt. Crystal structure of DPA_PA salt reveals the presence of a dimeric association between the protonated DPA molecule through the N–H···O hydrogen bond like DPA alone with different symmetry operation (Table 2 and Figure 8a). There is no direct association between the PA[−]–PA[−] anion observed in DPA_PA salt. However the protonated DPA molecule linked PA[−] anions alternatively through N–H···O, and charge assisted the N⁺–H···O[−] hydrogen bond shown in Figure 8b, in which one PA[−] anion associated with the protonated DPA molecule by forming the N–H···O hydrogen bond involving carbonyl C=O4 oxygen of the carboxyl group of PA[−] anion and amide N–H2A hydrogen of protonated DPA. Whereas the other PA[−] anion associated by forming a charge assisted N⁺–H···O[−] hydrogen bond by using carboxylate (COO[−]) O2-oxygen of the PA anion and the protonated tertiary amino group N3⁺–H3A hydrogen of protonated DPA; both associations were supported by C–H···O interaction as shown in Figure 8b.

In the crystal structure of DPA_PA salt, two inversion-symmetry related protonated DPA molecules form amide homodimer, via a pair of strong N2–H2B···O1 hydrogen bonds in R²₂(8) ring motif that involve two acceptor and two donor atoms. In this association, protonated DPA donates amide hydrogen N2–H2B to amide carbonyl (C=O1) oxygen of inversion-symmetry related protonated DPA molecules in dimeric N2–H2B···O1 hydrogen bonding interaction. Further, this amide homodimer of protonated DPA molecule linked to two PA anions through N2–H2A···O4 hydrogen bonding interaction between the second hydrogen of amide N2–H2A and carbonyl (C=O4) oxygen of the carboxyl group of the PA[−] anion and further supported by C9–H9···O4 interaction, between C9–H9 hydrogen of the phenyl ring of protonated DPA and carbonyl (C=O4) oxygen of the carboxyl group of the PA[−] anion resulting basic dimeric unit shown in Figure 9.

The dimeric unit linked to four *n*-glide related neighboring dimeric units through charge assisted strong and linear N⁺–H···O[−] hydrogen bonding interaction and supported by two longer and non-linear C–H···O[−] interactions, namely C17–H17A···O2[−], C14–H14B···O2[−] resulting 2-D packing. In this association, the carboxylate (COO[−]) O2-oxygen of PA[−] anion is made hydrogen bond with N3⁺–H3A (protonated tertiary amino nitrogen) hydrogen of protonated DPA via the charge assisted strong N3⁺–H3A···O2[−] hydrogen bond; such association was further supported by longer and non-linear C–H···O[−] interaction, namely C17–H17A···O2[−], C14–H14B···O2[−] interactions and resulting packing view down the *a*-axis is shown in Figure 10a (above). In this packing, the dimeric unit assembled along the *b*-axis through the short C2–H2···O1 hydrogen bond between amide carbonyl (C=O1) oxygen and C2–H2 hydrogen of 2-pyridine moieties of the next dimeric unit along the *b*-axis and supported by weak C18–H18A···C_g5 interaction between the C18–H18A hydrogen of *iso*-propyl moieties of protonated DPA and the π cloud of the

aromatic ring (C22-C23-C24-C25-C26-C27) of PA^- anion; the resulting association is shown in Figure 10a (down). Similar packing views in the ac -plane, reveal that the neighboring dimeric unit assembled along the ac -diagonal through hydrogen bonding, wherein there is an alternate arrangement of protonated DPA amide dimer and PA^- anion as shown in Figure 10b.

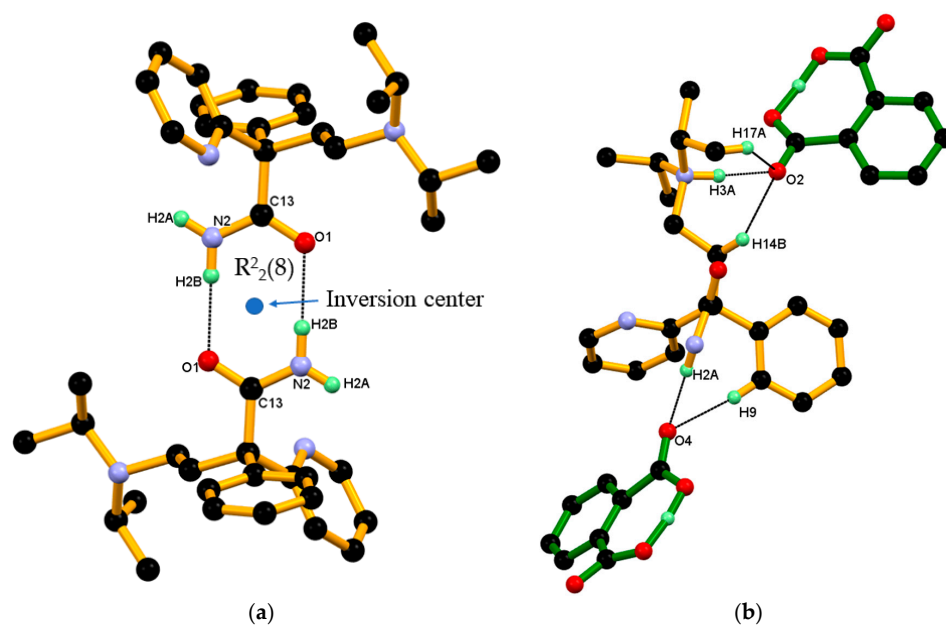


Figure 8. (a) Association between protonated DPA molecules through a pair of strong $\text{N-H}\cdots\text{O}$ hydrogen bonds in $R^2_2(8)$ ring motif; and (b) Association between the protonated DPA and PA^- anions in DPA-PA salt, hereby protonated DPA molecules engaging both carboxylate and carboxyl groups of the PA^- anion alternatively through a strong $\text{N-H}\cdots\text{O}$ and charge assisted $\text{N}^+-\text{H}\cdots\text{O}^-$ hydrogen bond and further supported by $\text{C-H}\cdots\text{O}$ interaction.

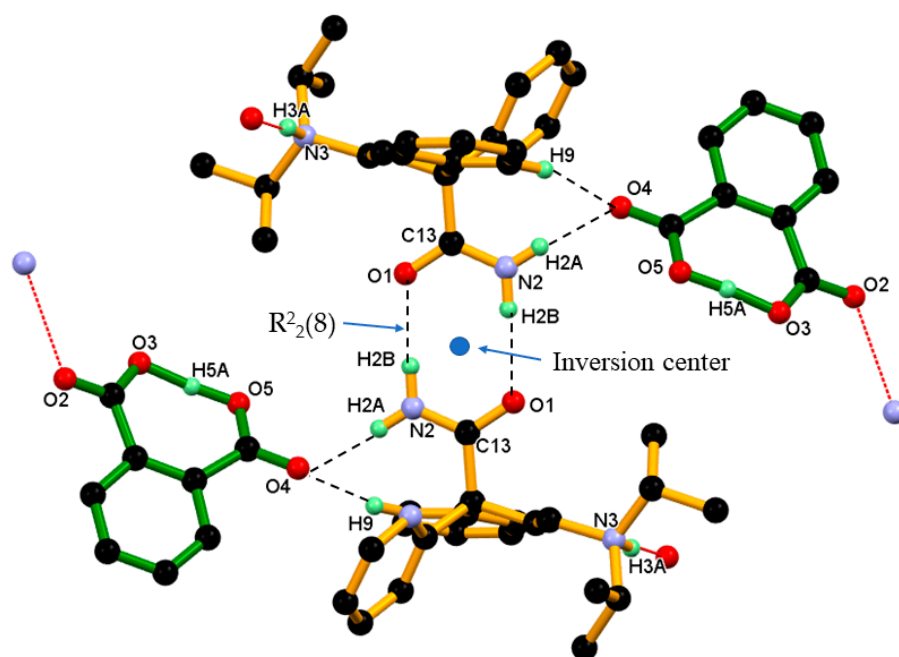
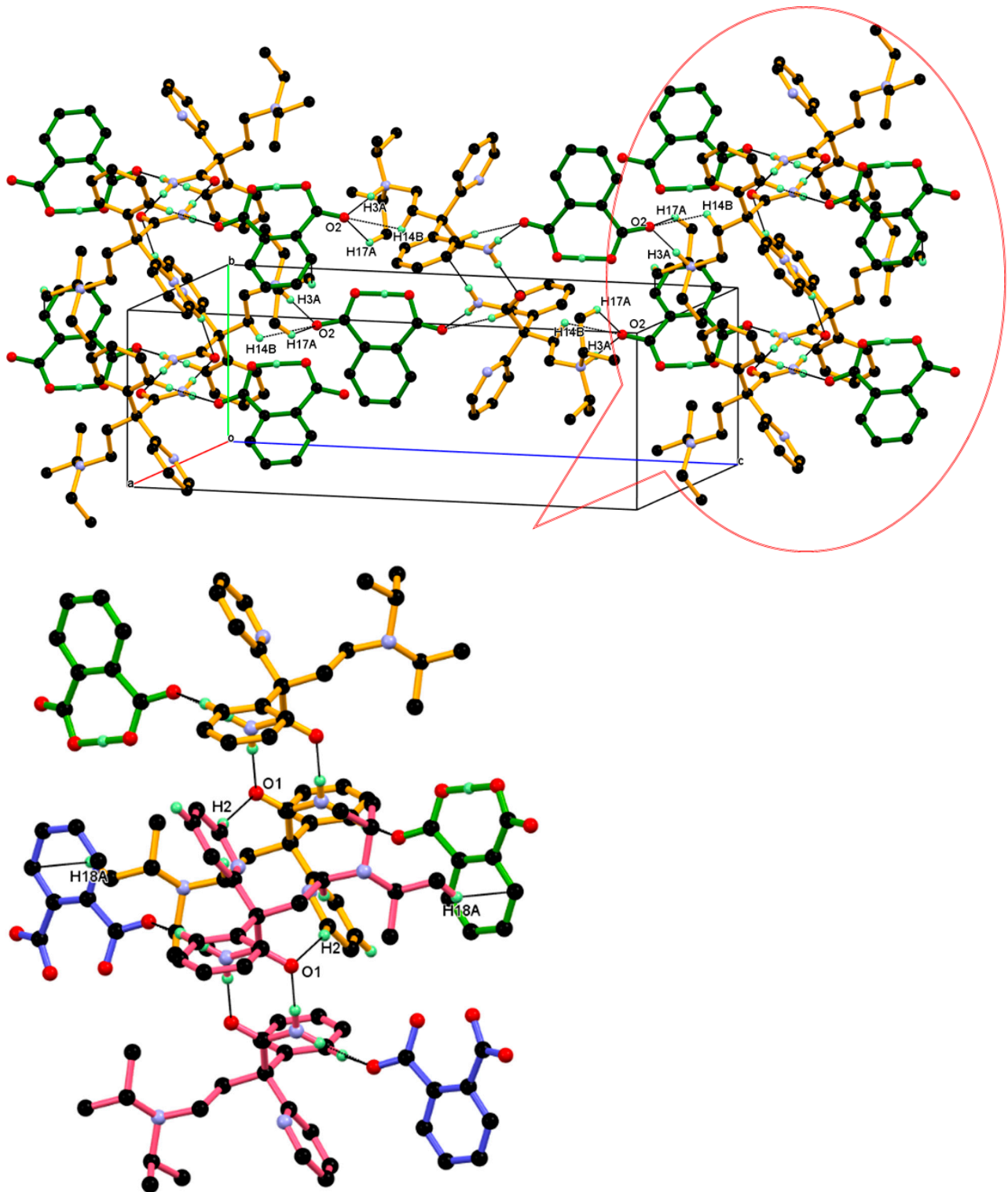


Figure 9. Dimeric unit of DPA-PA salt in crystal. Dotted lines indicate the non-covalent interaction (hydrogen atoms not involved in the hydrogen bonding were removed for clarity).



(a)

Figure 10. *Cont.*

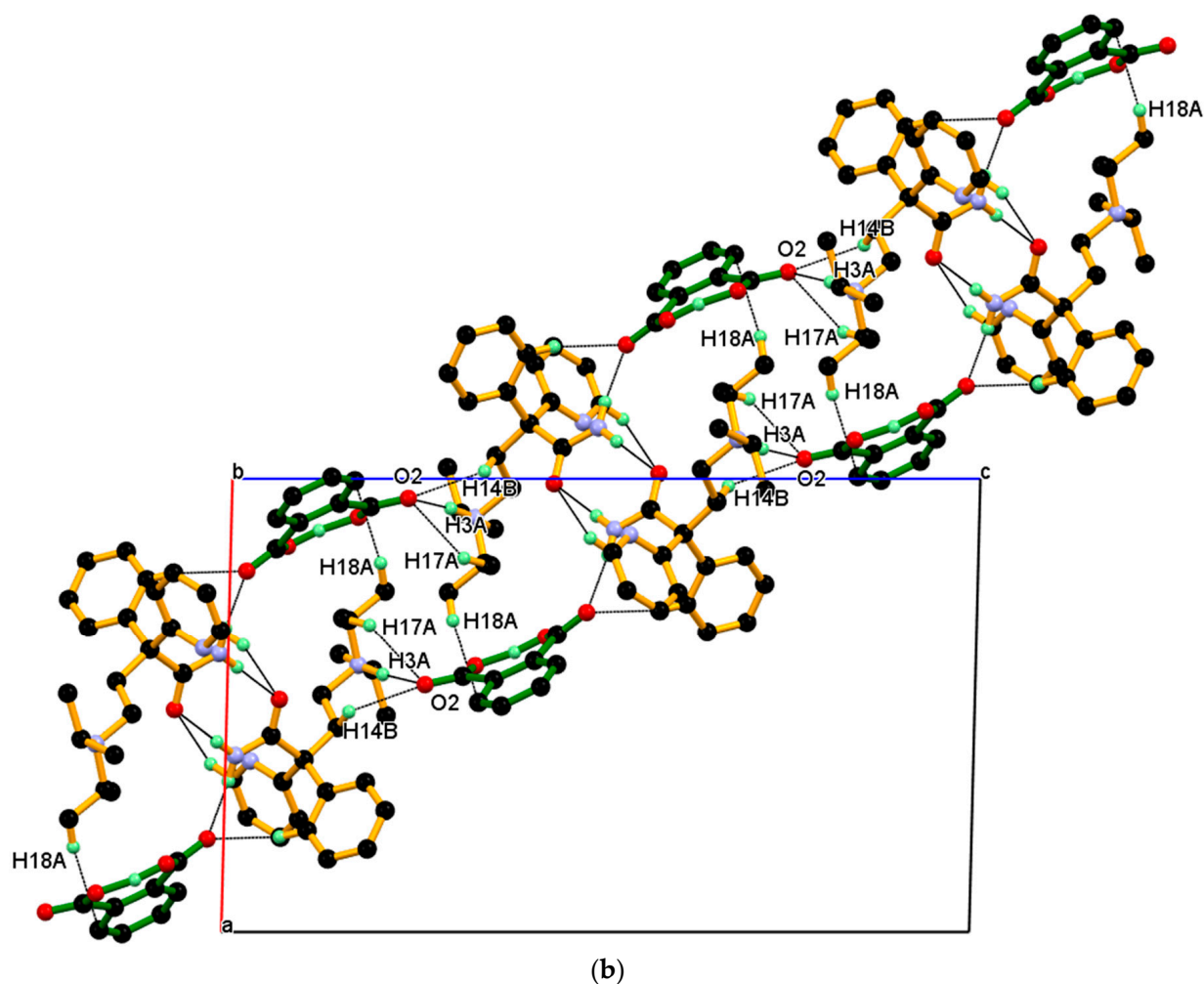


Figure 10. (a) Packing view down the *a*-axis, with each dimeric unit linked to four *n*-glide related neighboring dimeric units, resulting in 2-D packing (above). The inset shows the association between the neighboring dimeric unit shown in different colors through C2–H2...O1 interaction and supported by C18–H18A...C_g5 along the *b*-axis. (down) (b) Similar packing view in the *ac*-plane.

Further, such a two-dimensional network of dimeric unit assembled centrosymmetrically along the *a*-axis (parallel to the *ac*-diagonal) through longer and weak C11–H11...O2[−] interaction between C11–H11 hydrogen of the phenyl ring of protonated DPA and carboxylate (COO[−]) O2-oxygen of PA[−] anions resulting in three-dimensional packing of the dimeric unit in the *ac*-plane, as shown in Figure 11.

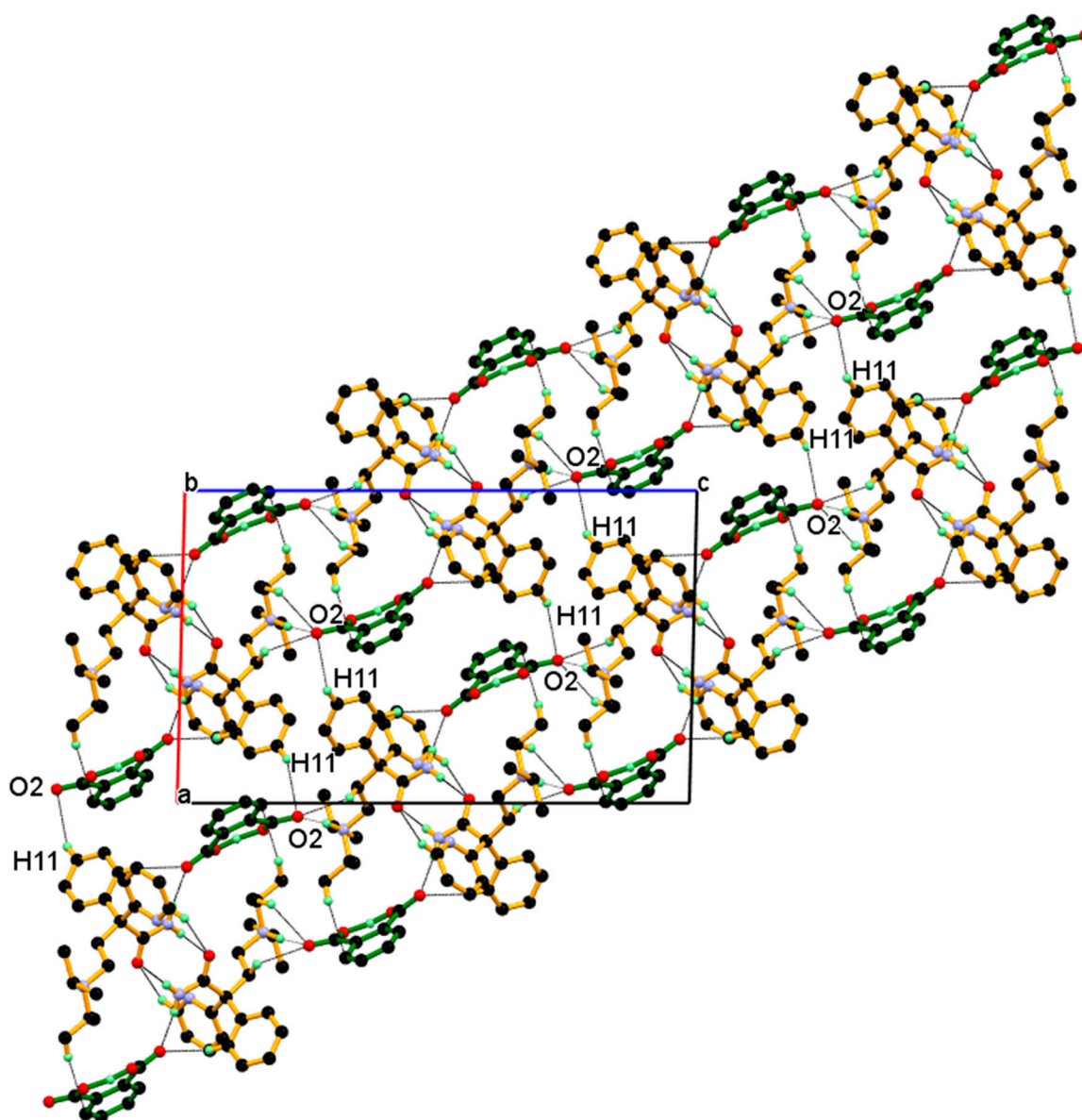


Figure 11. 2-Dimensional network of dimeric unit assembled centrosymmetric fashion through weak and longer C11-H11 \cdots O2 $^-$ interaction resulting in 3-D packing of dimeric unit in the *ac*-plane.

3.3. Structural Overlay

DPA (Figure 12a), has freely rotatable groups connected to asymmetric carbon marked by a star and anticipated to display conformational or orientational changes in its solid forms. The structural overlay of the DPA molecule by overlapping the (C-C-C-N) backbone chain, shown in Figure 12b, reveals conformational and orientational differences owing to rotational freedom around the C–C, C–N bonds. Conformational difference in both solid forms could be characterized by torsion angles τ_1 , τ_2 , τ_3 and τ_4 as shown in Figure 12a, and the dihedral angle between the phenyl and 2-pyridine moieties and values listed in Table 3. In pure DPA crystal structure, both conformers in the pure DPA crystal display slight difference in torsion angles τ_1 (–179.78, –171.37), while values of τ_2 (177.67, 177.17) and τ_3 (–1.01, 3.01) are comparable and indicate that the (C-C-C-N) backbone chain moiety connecting to the phenyl ring are nearly coplanar in molecule A, while there is a slight deviation observed in coplanarity in B molecules. On the other hand, the 2-pyridine ring is roughly perpendicular to the planar part of A and B molecules. The dihedral

angle between the phenyl and 2-pyridine rings is 87.16° and 79.83° in molecules A and B, respectively. In DPA_PA salt crystal structure, the torsion angles τ_1 and τ_2 are -177.58° , -175.47° suggesting coplanarity in the backbone chain as pure DPA, whereas torsion angles $\tau_3 -16.81^\circ$ indicate deviation in coplanarity in backbone chain moiety and the phenyl ring. Further, the dihedral angle between the phenyl and 2-pyridine moiety is significantly changed to 59.43° and such deviation in orientation of 2-pyridine and phenyl moiety could be due to the association of salt former (PA) with drug (DPA) through hydrogen bond in this direction. However, the torsional value τ_4 is for the orientation of the amide group with a planar part; it is nearly similar for both conformers in pure DPA, and such orientation of the amide group brings 2-pyridine moiety close enough to facilitate an intramolecular hydrogen bond between amide N-H hydrogen and N-atom of 2-pyridine moiety. Whereas in the DPA_PA salt a conformational twist is observed at amide group as shown in Figure 12b to facilitate the intermolecular hydrogen bond between amide N-H hydrogen of protonated DPA and carbonyl oxygen (C=O) of the carboxyl group PA⁻ anion. Moreover, *iso*-propyl moiety present on tertiary nitrogen in all molecules shows conformational/orientational difference.

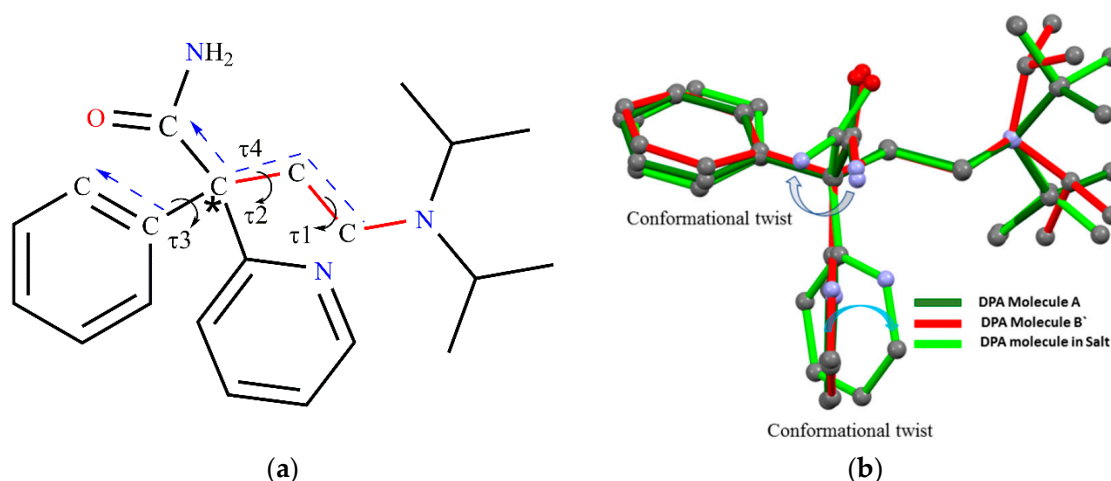


Figure 12. (a) Chemical structure of DPA, in which the (C-C-C-N) backbone chain is marked by a red color bond and (b) Structural overlay of DPA molecules in both solid forms showing significant conformational variation; Green-Molecule A, Red-Molecule B' in DPA, Light green-DPA molecules from DPA_PA salt.

Table 3. Torsional/dihedral angle in DPA and DPA_PA.

	τ_1°	τ_2°	τ_3°	τ_4°	Dihedral Angle $^\circ$
DPA Molecule A	-179.78	177.67	-1.01	63.83	87.16(6)
DPA Molecule B'	-171.37	177.17	3.12	63.90	79.83(6)
DPA from Salt	-177.60	-175.45	-16.81	69.39	59.43(7)

In DPA Molecule A: τ_1 —C7-C14-C15-N3, τ_2 —C6-C7-C14-C15, τ_3 —C1-C6-C7-C14, τ_4 —C13-C7-C14-C15; In DPA Molecule B': τ_1 —C28-C35-C36-N6, τ_2 —C27-C28-C35-C36, τ_3 —C22-C27-C28-C35, τ_4 —C34-C28-C35-C36; DPA from Salt: τ_1 —C7-C14-C15-N3, τ_2 —C8-C7-C14-C15, τ_3 —C4-C8-C7-C14, τ_4 —C13-C7-C14-C15. The dihedral angle is the angle between planes of the phenyl and 2-pyridine ring in DPA.

Crystal structure analysis showed that the drug–drug amide homosynthon retained in salt as in pure DPA (differed in symmetry operation). Further, the density of DPA alone and its salt DPA_PA calculated from single crystal X-ray diffraction were found to increase from 1.140 g/cm^3 in DPA to 1.269 g/cm^3 in the salt, indicating denser packing in salt.

3.4. Characterization of DPA and DPA_PA Salt

3.4.1. PXRD

The PXRD pattern recorded for commercially available DPA, DPA crystals, DPA_PA salt and PA. The PXRD pattern of the commercially available DPA and DPA crystal is

matched to reveal that both are in the same crystalline phase. Further PXRD patterns of the salt are different from individual components, suggesting formation of a new crystalline phase in the solid-state. (Figure S1). Furthermore, the overlapping of the experimental PXRD pattern of these crystals matched well the simulated PXRD pattern obtained from the single-crystal X-ray data, confirming the homogeneity of the sample.

3.4.2. FT-IR Spectrum

Considered as a reasonable and reliable technique to detect the formation of the multi-component crystal, Fourier transform infrared (FT-IR) spectroscopy is a very important tool to determine typical carboxylate anion and confirm the proton transfer when carboxylic acid is used as a coformer.

FT-IR spectra were obtained for commercial DPA, prepared DPA crystal, PA and DPA_PA salt (Figure S2). FT-IR spectrum of commercial DPA and prepared DPA crystal showed same characteristic peaks, which were observed as amide N-H stretching at 3263 cm^{-1} , amide C=O stretching and NH_2 deformation overlap peak at 1664 cm^{-1} , whereas in DPA_PA amide N-H stretching was observed at 3354.57 cm^{-1} , amide C=O stretch and NH_2 deformation at $1680, 1625\text{ cm}^{-1}$, respectively [58]. The blue shift of amide-derived peaks suggests the possible changes in the hydrogen bonding interaction between molecules due to the formation of a new solid form [59,60]. In general, for tertiary amine salts, a broad band at $2300\text{--}2700\text{ cm}^{-1}$ was due to the NH^+ stretching, which was also observed in DPA-PA salt, revealing the protonation of tertiary amine in DPA [60,61]. In addition, the peaks at 1590 and 1568 cm^{-1} in DPA were probably attributed to benzene and pyridine rings. It was observed that similar peaks appeared with minor differences in DPA_PA salt. Hence, it appears there is no chemical interaction on benzene and pyridine rings.

Due to the hydrogen bond of the PA dimer, pure PA existed over a broad band around 2800 cm^{-1} , attributed to the OH group, which shifts to 3191 cm^{-1} in DPA_PA salt. The carbonyl stretches of two carboxylic acid groups of PA were observed at 1666 and 1583 cm^{-1} , which appeared at 1679 cm^{-1} for the COOH group and 1556 cm^{-1} for the COO^- group in DPA-PA salt [62].

In short, the appearance of a broad band at $2300\text{--}2700\text{ cm}^{-1}$ and a peak at 1556 cm^{-1} , where the ionized tertiary amine and carboxylate group could be observed, respectively, indicate a proton transfer from the salt former PA to DPA, confirming the salt formation between DPA and PA.

3.4.3. Thermal Properties

The thermal properties of the DPA and DPA_PA salt were evaluated by DSC and TG measurements. DSC revealed a single sharp endotherm at $84\text{ }^\circ\text{C}$ in agreement with a reported metastable form at $85\text{ }^\circ\text{C}$. In the DSC curve of the DPA_PA salt, the endothermic peak at around $161\text{ }^\circ\text{C}$ is the melting point of salt, which is significantly different from DPA ($84\text{ }^\circ\text{C}$) and PA ($216\text{ }^\circ\text{C}$) (Figure S3). TG data of the DPA single crystal revealed that no weight loss before melting confirmed the absence of any solvent or hydrate in the crystal lattice as same as that of DPA commercial. Also, the thermal stability and decomposition processes of DPA_PA salt have been shown, measured by simultaneous TG in flowing air. The DPA_PA salt is stable until $160\text{ }^\circ\text{C}$ (Figure S4). There are no thermal moments for all crystals before the melting process, indicating that these crystals are unsolvated.

4. Conclusions

Pure DPA and its 1:1 DPA_PA salt crystals have been obtained from the slow solvent evaporation method and both belong to the centrosymmetric monoclinic crystal system having a $P2_1/n$ space group. The asymmetric unit of pure DPA contains two molecules while 1:1 DPA_PA salt contains one protonated DPA and one PA^- anion.

Crystal structure analysis of pure DPA showed two closely associated molecules formed amide–amide dimer through an $\text{N-H}\cdots\text{O}$ hydrogen bond and resulting in the $R^2_2(8)$

ring motifs. Dimeric units were assembled in the *ab*-plane through C-H \cdots O and C-H $\cdots\pi$ interaction, whereas it packed loosely along the *c*-axis via weak non-covalent interaction. Crystal structure analysis of 1: 1 DPA_PA salt showed a strong association between the drug and the salt former leading to compact molecular packing, with an increase in crystal density compared to DPA alone. In salt, two inversion symmetry related protonated DPA molecules formed amide homodimer through an N-H \cdots O hydrogen bond in R²₂(8) ring motifs and such dimer is hydrogen bonded to two PA[−] anions through N-H \cdots O and C-H \cdots O hydrogen bonds to form the basic dimeric unit comprising two protonated DPA and two PA[−] anion. Furthermore, dimeric units linked to four *n*-glide related neighboring dimeric units through a strong N⁺-H \cdots O[−] hydrogen bond resulted in a 2-Dimensional packing network. Such a 2-D network assembled in centrosymmetric fashion along the *a*-axis through weak C-H \cdots O interaction resulting 3-D packing in the *ac*-plane.

Supplementary Materials: The following are available online at <https://www.mdpi.com/article/10.3390/cryst11040379/s1>, Figure S1. PXRD patterns of (a) commercial DPA; (b) DPA crystal, (c) simulated DPA, (d) PA, (e) DPA_PA salt and (f) simulated DPA_PA salt, Figure S2. FT-IR spectra of (a) commercial DPA; (b) DPA crystal, (c) PA, (d) DPA_PA salt, Figure S3. DSC profiles of (a) commercial DPA, (b) DPA crystal, (c) PA, (d) DPA_PA, Figure S4. TG curves of commercial DPA (yellow), DPA crystal (gray), PA (orange), DPA_PA salt (blue).

Author Contributions: Conceptualization, Y.O., D.U., and O.D.P.; formal analysis, M.I.T., Y.O., D.U., O.D.P. and H.U.; investigation, Y.O., Y.U. and D.U.; writing of original draft preparation, M.I.T., T.F. and S.W.; writing of review and editing; T.F., O.D.P. and E.Y.; visualization, M.I.T., T.F., Y.U. and S.W.; supervision, T.F., O.D.P., K.F., H.U. and E.Y.; project administration, T.F., K.F. and E.Y. All authors have read and agreed to the published version of the manuscript.

Funding: Part of this work was supported by the Mochida Memorial Foundation for Medical and Pharmaceutical Research 2019–2020 (to T.F.) and JSPS KAKENHI Grant Number JP18H04504 and 20H04661 (to H.U.).

Acknowledgments: The authors are thankful to Takashi Kikuchi (Rigaku Corporation) for refining and solving the disorder in DPA_PA salt.

Conflicts of Interest: The authors declare no conflict of interest.

References

1. Brittain, H.G. *Polymorphism in Pharmaceutical Solids*; Taylor & Francis: London, UK, 1999.
2. Hilfiker, R.; von Raumer, M. *Polymorphism in the Pharmaceutical Industry: Solid Form and Drug Development*; Wiley: Hoboken, NJ, USA, 2019.
3. SeethaLekshmi, S.; Guru Row, T.N. Conformational Polymorphism in a Non-steroidal Anti-inflammatory Drug, Mefenamic Acid. *Cryst. Growth Des.* **2012**, *12*, 4283–4289. [[CrossRef](#)]
4. Babu, N.J.; Cherukuvada, S.; Thakuria, R.; Nangia, A. Conformational and Synthron Polymorphism in Furosemide (Lasix). *Cryst. Growth Des.* **2010**, *10*, 1979–1989. [[CrossRef](#)]
5. Li, L.; Yin, X.H.; Diao, K.S. Improving the Solubility and Bioavailability of Pemafibrate via a New Polymorph Form II. *ACS Omega* **2020**, *5*, 26245–26252. [[CrossRef](#)] [[PubMed](#)]
6. Karimi-Jafari, M.; Padrela, L.; Walker, G.M.; Croker, D.M. Creating Cocrystals: A Review of Pharmaceutical Cocrystal Preparation Routes and Applications. *Cryst. Growth Des.* **2018**, *18*, 6370–6387. [[CrossRef](#)]
7. Schultheiss, N.; Newman, A. Pharmaceutical Cocrystals and Their Physicochemical Properties. *Cryst. Growth Des.* **2009**, *9*, 2950–2967. [[CrossRef](#)] [[PubMed](#)]
8. Yousef, M.A.E.; Vangala, V.R. Pharmaceutical Cocrystals: Molecules, Crystals, Formulations, Medicines. *Cryst. Growth Des.* **2019**, *19*, 7420–7438. [[CrossRef](#)]
9. Gunnam, A.; Nangia, A.K. High-Solubility Salts of the Multiple Sclerosis Drug Teriflunomide. *Cryst. Growth Des.* **2019**, *19*, 5407–5417. [[CrossRef](#)]
10. Bezerra, B.P.; Pogoda, D.; Perry, M.L.; Vidal, L.M.T.; Zaworotko, M.J.; Ayala, A.P. Cocrystal Polymorphs and Solvates of the Anti-Trypanosoma cruzi Drug Benznidazole with Improved Dissolution Performance. *Cryst. Growth Des.* **2020**, *20*, 4707–4718. [[CrossRef](#)]
11. Berziņš, A.; Skarbulis, E.; Reķis, T.; Actiņš, A. On the Formation of Droperidol Solvates: Characterization of Structure and Properties. *Cryst. Growth Des.* **2014**, *14*, 2654–2664. [[CrossRef](#)]
12. Zvoníček, V.; Skořepová, E.; Dušek, M.; Babor, M.; Žvátora, P.; Šoóš, M. First Crystal Structures of Pharmaceutical Ibrutinib: Systematic Solvate Screening and Characterization. *Cryst. Growth Des.* **2017**, *17*, 3116–3127. [[CrossRef](#)]

13. Zhang, G.; Xiao, X.; Zhang, L.; Ren, G.; Zhang, S. Hydrates and Solvates of Acotiamide Hydrochloride: Crystallization, Structure, Stability, and Solubility. *Cryst. Growth Des.* **2018**, *19*, 768–779. [[CrossRef](#)]
14. Wang, K.; Wang, C.; Sun, C.C. Structural Insights into the Distinct Solid-State Properties and Interconversion of Celecoxib N-Methyl-2-pyrrolidone Solvates. *Cryst. Growth Des.* **2020**, *21*, 277–286. [[CrossRef](#)]
15. Sathisaran, I.; Dalvi, S.V. Engineering Cocrystals of Poorly Water-Soluble Drugs to Enhance Dissolution in Aqueous Medium. *Pharmaceutics* **2018**, *10*, 108. [[CrossRef](#)] [[PubMed](#)]
16. Banerjee, R.; Bhatt, P.M.; Ravindra, N.V.; Desiraju, G.R. Saccharin Salts of Active Pharmaceutical Ingredients, Their Crystal Structures, and Increased Water Solubilities. *Cryst. Growth Des.* **2005**, *5*, 2299–2309. [[CrossRef](#)]
17. Shan, N.; Perry, M.L.; Weyna, D.R.; Zaworotko, M.J. Impact of pharmaceutical cocrystals: The effects on drug pharmacokinetics. *Expert Opin. Drug Metab. Toxicol.* **2014**, *10*, 1255–1271. [[CrossRef](#)]
18. Swapna, B.; Maddileti, D.; Nangia, A. Cocrystals of the Tuberculosis Drug Isoniazid: Polymorphism, Isostructurality, and Stability. *Cryst. Growth Des.* **2014**, *14*, 5991–6005. [[CrossRef](#)]
19. Guo, C.; Zhang, Q.; Zhu, B.; Zhang, Z.; Bao, J.; Ding, Q.; Ren, G.; Mei, X. Pharmaceutical Cocrystals of Nicorandil with Enhanced Chemical Stability and Sustained Release. *Cryst. Growth Des.* **2020**, *20*, 6995–7005. [[CrossRef](#)]
20. Nechipadappu, S.K.; Reddy, I.R.; Tarafder, K.; Trivedi, D.R. Salt/Cocrystal of Anti-Fibrinolytic Hemostatic Drug Tranexamic acid: Structural, DFT, and Stability Study of Salt/Cocrystal with GRAS Molecules. *Cryst. Growth Des.* **2018**, *19*, 347–361. [[CrossRef](#)]
21. Thakur, T.S.; Thakuria, R. Crystalline Multicomponent Solids: An Alternative for Addressing the Hygroscopicity Issue in Pharmaceutical Materials. *Cryst. Growth Des.* **2020**, *20*, 6245–6265. [[CrossRef](#)]
22. Chen, Y.; Li, L.; Yao, J.; Ma, Y.-Y.; Chen, J.-M.; Lu, T.-B. Improving the Solubility and Bioavailability of Apixaban via Apixaban–Oxalic Acid Cocrystal. *Cryst. Growth Des.* **2016**, *16*, 2923–2930. [[CrossRef](#)]
23. Zhu, B.; Zhang, Q.; Wang, J.-R.; Mei, X. Cocrystals of Baicalein with Higher Solubility and Enhanced Bioavailability. *Cryst. Growth Des.* **2017**, *17*, 1893–1901. [[CrossRef](#)]
24. Mannava, M.K.C.; Suresh, K.; Nangia, A. Enhanced Bioavailability in the Oxalate Salt of the Anti-Tuberculosis Drug Ethionamide. *Cryst. Growth Des.* **2016**, *16*, 1591–1598. [[CrossRef](#)]
25. Desiraju, G.R. Supramolecular Synthons in Crystal Engineering—A New Organic Synthesis. *Angew. Chem. Int. Ed. Engl.* **1995**, *34*, 2311–2327. [[CrossRef](#)]
26. Corpinot, M.K.; Bučar, D.-K. A Practical Guide to the Design of Molecular Crystals. *Cryst. Growth Des.* **2018**, *19*, 1426–1453. [[CrossRef](#)]
27. Desiraju, G.R. *Crystal Engineering: The Design of Organic Solids*; Elsevier: Amsterdam, The Netherlands, 1989.
28. Berry, D.J.; Steed, J.W. Pharmaceutical cocrystals, salts and multicomponent systems; intermolecular interactions and property based design. *Adv. Drug Deliv. Rev.* **2017**, *117*, 3–24. [[CrossRef](#)] [[PubMed](#)]
29. Martins, I.C.B.; Sardo, M.; Santos, S.M.; Fernandes, A.; Antunes, A.; André, V.; Mafra, L.; Duarte, M.T. Packing Interactions and Physicochemical Properties of Novel Multicomponent Crystal Forms of the Anti-Inflammatory Azelaic Acid Studied by X-ray and Solid-State NMR. *Cryst. Growth Des.* **2015**, *16*, 154–166. [[CrossRef](#)]
30. Lin, B.; Liu, Y.; Wang, M.; Wang, Y.; Du, S.; Gong, J.; Wu, S. Intermolecular Interactions and Solubility Behavior of Multicomponent Crystal Forms of Orotic Acid: Prediction and Experiments. *Cryst. Growth Des.* **2021**. [[CrossRef](#)]
31. Rajput, L.; Sanphui, P.; Desiraju, G.R. New Solid Forms of the Anti-HIV Drug Etravirine: Salts, Cocrystals, and Solubility. *Cryst. Growth Des.* **2013**, *13*, 3681–3690. [[CrossRef](#)]
32. George, C.P.; Thorat, S.H.; Shaligram, P.S.; Gonnade, R.G. Drug–drug cocrystals of anticancer drugs erlotinib–furosemide and gefitinib–mefenamic acid for alternative multi-drug treatment. *Cryst. Eng. Comm.* **2020**, *22*, 6137–6151. [[CrossRef](#)]
33. Nangia, A.K.; Desiraju, G.R. Crystal Engineering: An Outlook for the Future. *Angew. Chem. Int. Ed. Engl.* **2019**, *58*, 4100–4107. [[CrossRef](#)]
34. Desiraju, G.R. Crystal engineering: From molecule to crystal. *J. Am. Chem. Soc.* **2013**, *135*, 9952–9967. [[CrossRef](#)]
35. Mir, N.A.; Dubey, R.; Desiraju, G.R. Strategy and Methodology in the Synthesis of Multicomponent Molecular Solids: The Quest for Higher Cocrystals. *Acc. Chem. Res.* **2019**, *52*, 2210–2220. [[CrossRef](#)]
36. Sarkar, N.; Sinha, A.S.; Aakeröy, C.B. Systematic investigation of hydrogen-bond propensities for informing co-crystal design and assembly. *Cryst. Eng. Comm.* **2019**, *21*, 6048–6055. [[CrossRef](#)]
37. Chu, Q.; Duncan, A.J.E.; Papaefstathiou, G.S.; Hamilton, T.D.; Atkinson, M.B.J.; Mariappan, S.V.S.; MacGillivray, L.R. Putting Cocrystal Stoichiometry to Work: A Reactive Hydrogen-Bonded “Superassembly” Enables Nanoscale Enlargement of a Metal–Organic Rhomboid via a Solid-State Photocycloaddition. *J. Am. Chem. Soc.* **2018**, *140*, 4940–4944. [[CrossRef](#)]
38. Ericson, D.P.; Zurfluh-Cunningham, Z.P.; Groeneman, R.H.; Elacqua, E.; Reinheimer, E.W.; Noll, B.C.; MacGillivray, L.R. Regiocontrol of the [2 + 2] Photodimerization in the Solid State Using Isosteric Resorcinols: Head-to-Tail Cyclobutane Formation via Unexpected Embraced Assemblies. *Cryst. Growth Des.* **2015**, *15*, 5744–5748. [[CrossRef](#)]
39. Katz, M.J.; Meyer, C.E.; El-Etr, A.; Slodki, S.J. Clinical evaluation of a new anti-arrhythmic agent, SC-7031. *Curr. Ther. Res. Clin. Exp.* **1963**, *5*, 343–350.
40. Rizos, I.; Brachmann, J.; Lengfelder, W.; Schmitt, C.; von Olshausen, K.; Kubler, W.; Senges, J. Effects of intravenous disopyramide and quinidine on normal myocardium and on the characteristics of arrhythmias: Intraindividual comparison in patients with sustained ventricular tachycardia. *Eur. Heart J.* **1987**, *8*, 154–163. [[CrossRef](#)]

41. Kim, S.Y.; Benowitz, N.L. Poisoning due to class IA antiarrhythmic drugs. Quinidine, procainamide and disopyramide. *Drug Saf.* **1990**, *5*, 393–420. [[CrossRef](#)]
42. Gunning, S.R.; Freeman, M.; Stead, J.A. Polymorphism of disopyramide. *J. Pharm. Pharmacol.* **1976**, *28*, 758–761. [[CrossRef](#)] [[PubMed](#)]
43. Kawamura, T.; Hirayama, N. Crystal structure of α -diisopropylaminoethyl- α -phenylpyridine-2-Acetamide phosphate, [C₂₁H₃₀N₃O] [H₂PO₄]. *Z. Krist. N. Cryst. Struct.* **2011**, *226*, 479. [[CrossRef](#)]
44. Burke, T.R., Jr.; Nelson, W.L.; Mangion, M.; Hite, G.J.; Mokler, C.M.; Ruenitz, P.C. Resolution, absolute configuration, and antiarrhythmic properties of the enantiomers of disopyramide, 4-(diisopropylamino)-2-(2-pyridyl)-2-phenylbutyramide. *J. Med. Chem.* **1980**, *23*, 1044–1048. [[CrossRef](#)] [[PubMed](#)]
45. Putra, O.D.; Pettersen, A.; Nilsson Lill, S.O.; Umeda, D.; Yonemochi, E.; Nugraha, Y.P.; Uekusa, H. Capturing a new hydrate polymorph of amodiaquine dihydrochloride dihydrate via heterogeneous crystallisation. *Cryst. Eng. Comm.* **2019**, *21*, 2053–2057. [[CrossRef](#)]
46. Putra, O.D.; Furuishi, T.; Yonemochi, E.; Terada, K.; Uekusa, H. Drug–Drug Multicomponent Crystals as an Effective Technique to Overcome Weaknesses in Parent Drugs. *Cryst. Growth Des.* **2016**, *16*, 3577–3581. [[CrossRef](#)]
47. Nagase, H.; Kobayashi, M.; Ueda, H.; Furuishi, T.; Gunji, M.; Endo, T.; Yonemochi, E. Crystal Structure of an Epalrestat Dimethanol Solvate. *X Ray Struct. Anal. Online* **2016**, *32*, 7–9. [[CrossRef](#)]
48. Putra, O.D.; Umeda, D.; Nugraha, Y.P.; Furuishi, T.; Nagase, H.; Fukuzawa, K.; Uekusa, H.; Yonemochi, E. Solubility improvement of epalrestat by layered structure formation via cocrystallization. *Cryst. Eng. Comm.* **2017**, *19*, 2614–2622. [[CrossRef](#)]
49. Hata, N.; Furuishi, T.; Tamboli, M.I.; Ishizaki, M.; Umeda, D.; Fukuzawa, K.; Yonemochi, E. Crystal Structural Analysis of DL-Mandelate Salt of Carvedilol and Its Correlation with Physicochemical Properties. *Crystals* **2020**, *10*, 53. [[CrossRef](#)]
50. Higashi, T. *Calculated Using ABSCOR. Empirical Absorption Correction Based on Fourier Series Approximation*; Rigaku: The Woodland, TX, USA, 1994.
51. Messerschmidt, A.; Schneider, M.; Huber, R. ABSCOR: A scaling and absorption correction program for the FAST area detector diffractometer. *J. Appl. Crystallogr.* **1990**, *23*, 436–439. [[CrossRef](#)]
52. Burla, M.C.; Caliandro, R.; Camalli, M.; Carrozzini, B.; Cascarano, G.L.; De Caro, L.; Giacovazzo, C.; Polidori, G.; Spagna, R. SIR2004: An improved tool for crystal structure determination and refinement. *J. Appl. Crystallogr.* **2005**, *38*, 381–388. [[CrossRef](#)]
53. Sheldrick, G.M. A short history of SHELX. *Acta Crystallographica. Sect. Found. Crystallogr.* **2008**, *64*, 112–122. [[CrossRef](#)]
54. Macrae, C.F.; Bruno, I.J.; Chisholm, J.A.; Edgington, P.R.; McCabe, P.; Pidcock, E.; Rodriguez-Monge, L.; Taylor, R.; van de Streek, J.; Wood, P.A. Mercury CSD 2.0—New features for the visualization and investigation of crystal structures. *J. Appl. Crystallogr.* **2008**, *41*, 466–470. [[CrossRef](#)]
55. Mittapalli, S.; Mannava, M.K.C.; Sahoo, R.; Nangia, A. Cocrystals, Salts, and Supramolecular Gels of Nonsteroidal Anti-Inflammatory Drug Niflumic Acid. *Cryst. Growth Des.* **2018**, *19*, 219–230. [[CrossRef](#)]
56. Kavanagh, O.N.; Walker, G.; Lusi, M. Graph-Set Analysis Helps to Understand Charge Transfer in a Novel Ionic Cocrystal When the ΔpK_a Rule Fails. *Cryst. Growth Des.* **2019**, *19*, 5308–5313. [[CrossRef](#)]
57. Chen, X.; Li, D.; Deng, Z.; Zhang, H. Ketoconazole: Solving the Poor Solubility via Cocrystal Formation with Phenolic Acids. *Cryst. Growth Des.* **2020**, *20*, 6973–6982. [[CrossRef](#)]
58. Wickman, A.; Finnegan, P. Disopyramide Phosphate. In *Analytical Profiles of Drug Substances*; Florey, K., Ed.; Academic Press: New York, NY, USA, 1984; Volume 13, pp. 183–209.
59. Brittain, H.G. Vibrational Spectroscopic Studies of Cocrystals and Salts. 1. The Benzamide–Benzoic Acid System. *Crystal Growth Des.* **2009**, *9*, 2492–2499. [[CrossRef](#)]
60. Brittain, H.G. Vibrational Spectroscopic Studies of Cocrystals and Salts. 2. The Benzylamine–Benzoic Acid System. *Cryst. Growth Des.* **2009**, *9*, 3497–3503. [[CrossRef](#)]
61. Smith, B.C. Organic nitrogen compounds V: Amine salts. *Spectroscopy* **2019**, *34*, 30–37.
62. Kundu, S.; Kumari, N.; Soni, S.R.; Ranjan, S.; Kumar, R.; Sharon, A.; Ghosh, A. Enhanced Solubility of Telmisartan Phthalic Acid Cocrystals within the pH Range of a Systemic Absorption Site. *ACS Omega* **2018**, *3*, 15380–15388. [[CrossRef](#)] [[PubMed](#)]